J Nanopart Res (2013) 15:1872
DOI 10.1007/s11051-013-1872-2

RESEARCH PAPER

Ge nanoparticles by direct oxidation of Zintl alloys and their electrochemical behavior as anodes of Li-ion batteries

Mathilde Pelosi · Monique Tillard · David Zitoun

Received: 28 May 2013 / Accepted: 15 July 2013

Abstract Germanium nanoparticles (NPs) are obtained by direct oxidation of a solid-state $Na_{12}Ge_{17}$ Zintl phase used as germanium precursor. Alcohols are chosen as oxidizing agents in a room-temperature process. The materials are characterized by X-ray diffraction, transmission electron microscopy, and Raman spectroscopy. The nature of the alcohol influences the final products and their crystallinity. The germanium NPs, tested as anodic materials for lithium ion batteries, display interesting behaviors with initial capacities up to 1,530 mAh g^{-1}.

Keywords Germanium · Nanocrystals · Nanoparticles · Li-ion · Battery

M. Pelosi · M. Tillard (✉) · D. Zitoun (✉)
Agrégats, Interfaces et Matériaux pour l'Energie, Institut Charles Gerhardt, CNRS UM2, UMR 5253, CC015, Université de Montpellier II, Sciences et Techniques du Languedoc, 2 Place Eugène Bataillon, 34095 Montpellier Cedex 5, France
e-mail: mtillard@univ-montp2.fr

D. Zitoun
e-mail: david.zitoun@biu.ac.il

D. Zitoun
Department of Chemistry, Bar Ilan Institute of Nanotechnology and Advanced Materials, Bar-Ilan University, 52900 Ramat Gan, Israel

Introduction

Germanium nanoparticles (NPs) have attracted attention as potential competitors for optoelectronic devices, elaborated by a bottom-up approach. Nanocrystals of germanium have also been studied for the quantum size effect on their optical properties (Heath et al. 1994; Bostedt et al. 2004). Elemental Ge has important applications in transistors, photodetectors, sensors, and batteries. As anodic material for Li-ion batteries, germanium displays a high theoretical capacity (1,600 mAh g^{-1}) and allows faster lithium diffusivity than silicon (extrapolated to be 400 times higher at room temperature) (Fuller and Severiens 1954). Nevertheless, the use of group 14 elements like Ge, Si, or Sn in anodes has been hampered by the poor cyclability of bulk materials, a drawback that could be overcome at the nanometric scale (Armand and Tarascon 2008). The success in colloidal bottom-up approach synthesis of Ge is more limited than the textbook examples of II–VI and even IV–VI and III–V semiconductors and synthesis pathways deserve further investigations.

Gas-phase syntheses have been reported for the preparation of well-defined germanium nanocrystals (Medeiros-Ribeiro et al. 1998; Min et al. 1996) and nanowires (Morales and Lieber 1998; Wu and Yang 2000; Wang and Dai 2002, 2006; Wang et al. 2005). The common precursors used in chemical vapor deposition are germanes (like Ge_2H_6), chlorogermanes, or phenylgermanes, which undergo thermal

Published online: 30 July 2013

decomposition or hydrogenolysis; in the presence of a metal catalyst, Vapor–Liquid–Solid mechanism leads to the formation of anisotropic nanostructure. These routes have been adapted to the synthesis of Ge nanocrystals in high boiling point solvents (Gerion et al. 2004; Zaitseva et al. 2007; Chockla et al. 2011) or supercritical fluids (Lu et al. 2004; Collins et al. 2010) and to Solution–Liquid–Solid mechanism toward the formation of Ge nanorods (Hanrath and Korgel 2002; Lu et al. 2005a, b).

Examples of solution routes are sparser and involve the reduction of a germanium halide ($GeCl_4$ and $RGeCl_3$) by a strong reducing agent alkalides (Heath et al. 1994), butyl-lithium, naphthalides (Kornowski et al. 1993; Chiu and Kauzlarich 2006), or hydrides (Wilcoxon et al. 2001; Chou et al. 2009), in the presence of a surfactant to limit the NPs growth and coalescence. Very recently, oleylamine has been successfully used as reducing agent in a microwave-assisted synthesis of Ge NPs (Muthuswamy et al. 2013). Alternative routes consist in the thermal decomposition of chlorogermane (Henderson et al. 2008), germanium alkoxide (Gerung et al. 2006), or $Ge\{N(SiMe)_3\}_2$ (Lambert et al. 2007; Gerung et al. 2005). As shown recently, the use of GeI_4 and/or GeI_2 as precursors allowed a better control over the particle mean size and the size dispersion of the colloidal product (Lu et al. 2005b; Ruddy et al. 2010; Vaughn et al. 2010). The stable colloidal suspension is suitable for spectroscopic studies (Lee et al. 2009) but the surfactant shell impedes its use for electronic/electrochemical applications.

Therefore, the use of germanium Zintl phases (Ge anionic clusters with alkaline or alkaline earth cations) has been standing as a unique room-temperature oxidative route toward Ge nanostructures. The Kauzlarich group has first developed this pathway by varying the Zintl phase (NaGe, KGe, and Mg_2Ge), the oxidative agent $GeCl_4$ or $GeCl_2$, and the capping agent (Grignard reagent or alkyl lithium) (Ma et al. 2008; Taylor et al. 1998, 1999, 2002; Tanke et al. 2003; Chiu et al. 2005). Such Zintl precursors have been successfully used as building blocks for Ge mesoporous materials (Armatas and Kanatzidis 2006a, b; Sun et al. 2006) and anodic materials for Li-ion batteries (Lee et al. 2005; Park et al. 2010). Soft oxidation of Zintl phases also yields a guest-free clathrate and an allotropic form (metastable *allo*-Ge) of germanium (Guloy et al. 2006; Gruttner et al. 1982; Kiefer et al. 2011). The appealing ability to perform a room-temperature synthesis of germanium nanostructures starting from Zintl precursors, and the need for better comprehension of the reaction pathways, drive us to study the reactivity of germanium anionic clusters under oxidation with mild reducing agents.

In this paper, we report on the preparation of Ge NPs by direct oxidation of Ge Zintl anions by alcohols. The $Na_{12}Ge_{17}$ Zintl phase has been used as germanium precursor either in solid state or after dissolution in ethylenediamine. Transmission electron microscopy (TEM) shows that the chain length of the alcohol and the reaction pathway have some influence on the mean size, the crystallinity, and the size dispersion of particles. The crystallinity has been carefully studied by Raman spectroscopy. The electrochemical tests of NPs as anodic materials for Li-ion batteries emphasize the relationship between synthesis pathway and properties.

Experimental section

Reagents are handled in a glove box under controlled argon atmosphere. Before the reaction with Ge powder (150 μm, Sigma Aldrich, 99.999 %), the alkali metal (Na, ingots, Merck, >99 %) is scraped to remove surface impurities. Benzyl alcohol ($C_6H_5CH_2OH$, 99 %, anhydrous, Acros-Organics) is used without further purification and anhydrous *n*-butanol (C_4H_9OH, Sigma Aldrich) is dried on a Schlenk line. The Zintl phase $Na_{12}Ge_{17}$ is prepared from stoichiometric proportions of the elements mixed in a weld-sealed Ta-container, enclosed in its turn within an evacuated silica or stainless steel jacket to avoid any oxidation at high temperature. The Na/Ge mixture is heated to 1,230 K for 2 days during which the reactor is shaken several times to improve homogenization of the melt. The air-sensitive products of reactions are handled in the glove box.

NPs are obtained by direct oxidation of the solid precursor by an alcohol. In such a reaction, called route I reaction, the alcohol is acting as oxidizing agent as well as solvent. The $Na_{12}Ge_{17}$ powder (100 mg) is slowly added to 10 mL alcohol under stirring in a glove box or on a vacuum line. The reaction time is optimized for completion of the reaction, and the solution is left to stir for 16 h, a time beyond which no homogeneity improvement in the

product is observed. At the end of the reaction, the black powder (Ge NPs) is separated by centrifugation and washed with hexane.

NPs are also obtained from a different pathway in the route II reaction: the solid $Na_{12}Ge_{17}$ (100 mg) is initially dissolved in ethylenediamine (10 mL) before adding the alcohol (10 mL). For this alternate route, the total reaction time should be divided into two parts: the time required for the solubilization which is set to 72 h and the oxidation time which is fixed to 16 h (as in the route I reaction). Temperature change from 273 to 473 K has no noticeable effect on the reaction products; therefore, all the experiments are carried out at room temperature.

A modified pathway named route III is used in order to avoid the high-temperature synthesis of the Zintl phase. The elements, Na and Ge, were taken in 12/17 atomic proportions and directly mixed in ethylenediamine before the oxidation reaction.

Note that similar reactions are successfully carried out starting from K_4Ge_9, a Zintl phase having a weaker reducing character (attributed to the weaker negative mean charge per Ge atom Goicoechea and Sevov 2005) and consequently a lower reactivity toward the alcohol.

TEM is performed with a JEOL 1200 EX II microscope operating at 100 kV accelerating voltage. The X-ray diffraction (XRD) patterns are recorded on a Philips analytical X'pert diffractometer equipped with a copper tube and a hybrid monochromator (parabolic multilayer mirror and two-crystal, Cu Kα radiation). The Raman spectroscopy is carried out using a LAbRam Aramis IR^2 spectrometer equipped with a helium neon laser (633 nm). The intensity of the laser beam is estimated to a maximal value of 6 mW very close to the sample. The use of various filters (named D0.6, D1, and D2) allows a reduction of intensity to 200, 70, and 50 μW, respectively.

The electrochemical behavior of nanostructured Ge powders is evaluated in Li/$LiPF_6$ (EC, PC, DMC)/Ge electrochemical cells assembled under argon in a glove box. Electrodes incorporated 85 wt.% active material intimately mixed with 15 wt.% carbon black. A 1 M solution of $LiPF_6$ in a 1:1:3-mixture of ethyl, propyl, and dimethyl carbonates (Merck Laboratories) is used as electrolyte. Charge–discharge experiments are monitored in standard conditions using a MacPile multichannel galvanostat–potentiostat. Li insertion/extraction is limited within a 0–2.5 V (vs. Li^+/Li) window voltage. The polarization between charge and discharge voltage upon cycling did not exceed 0.5 V. The voltage versus composition curves are plotted for the first cycles of galvanostatic experiments performed at a regime corresponding to the exchange of one Li atom in 10 h.

Results and discussion

Ge NPs have been prepared from the oxidation of a Zintl phase used as Ge precursor (Fig. 1). Alcohols are chosen as oxidizing agents for their especially mild reducing character. Furthermore, they can be easily removed from the nanostructure surface after synthesis. The alcoholic proton reacts with the Zintl phase to give gaseous H_2 and alkoxide (which protonates upon reaction in air). Indeed, the reaction occurs with gas evolution and no other by product has been noticed from ^1H NMR spectrum of the supernatants.

The route I reaction is a direct oxidation of the solid phase by a liquid oxidant also acting as solvent. Instead, route II reaction takes advantage of the special property of Ge Zintl phases to be soluble in basic polar solvents, as for example ethylenediamine. Solubilization releases free Zintl anions in the solution that are ready to react directly with the oxidant in the liquid phase.

Precursor characterization

The solid Zintl phase $Na_{12}Ge_{17}$ is prepared from the elements by high-temperature synthesis. The profile refinement of its experimental XRD powder pattern

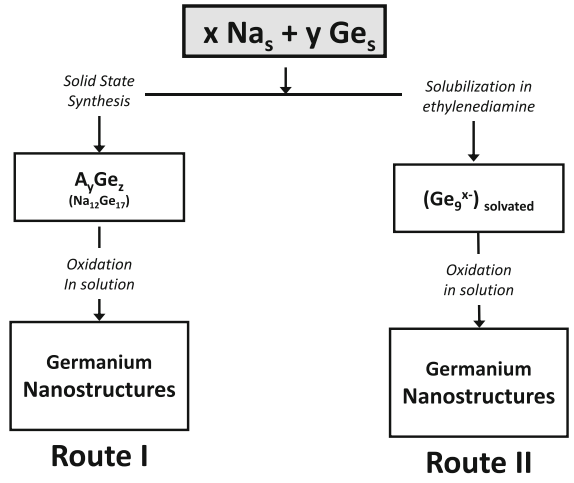

Fig. 1 Schematic representation of the synthetic routes I and II

(Rietveld procedure in program Jana) leads to good agreement factors R_p/R_{wp} of 1.1/1.8 % (Fig. 2a). Parameters of the monoclinic unit cell ($P2_1/c$) converge to $a = 22.095(2)$, $b = 12.8090(6)$, $c = 41.580(2)$ Å, $\beta = 91.341(2)°$, values that agree well with those previously reported (Taylor et al. 1998): $a = 22.11$, $b = 12.80$, $c = 41.56$ Å, $\beta = 91.3°$. The structure of $Na_{12}Ge_{17}$ is characterized by the coexistence of two discrete anionic units, Ge_4^{4-} and Ge_9^{4-}, packed together with sodium cations (Fig. 2c). Then, the $Na_{12}Ge_{17}$ Zintl compound can be formally described as $[Na^+]_{12}$ $[Ge_4^{4-}]_2$ $[Ge_9^{4-}]$.

Raman spectroscopy is a complementary technique for the full identification of $Na_{12}Ge_{17}$. According to literature reports (Hoch et al. 2003; Kliche et al. 1992; Somer 2000), Ge_4^{4-} unit (symmetry Td) is characterized by three Raman active vibration modes observed at 274 cm^{-1} (ν_1), 207 cm^{-1} (ν_2), and 164 cm^{-1} (ν_3). For Ge_9^{4-} anion displaying the C_{4v} symmetry, only five out of the 20 active modes are observed at 222 cm^{-1} (intense), 164 and 167 cm^{-1} (medium), and 241 and 188 cm^{-1} (weak).

The Raman spectrum recorded for $Na_{12}Ge_{17}$ is composed of three bands (Fig. 2b), those at 276 and

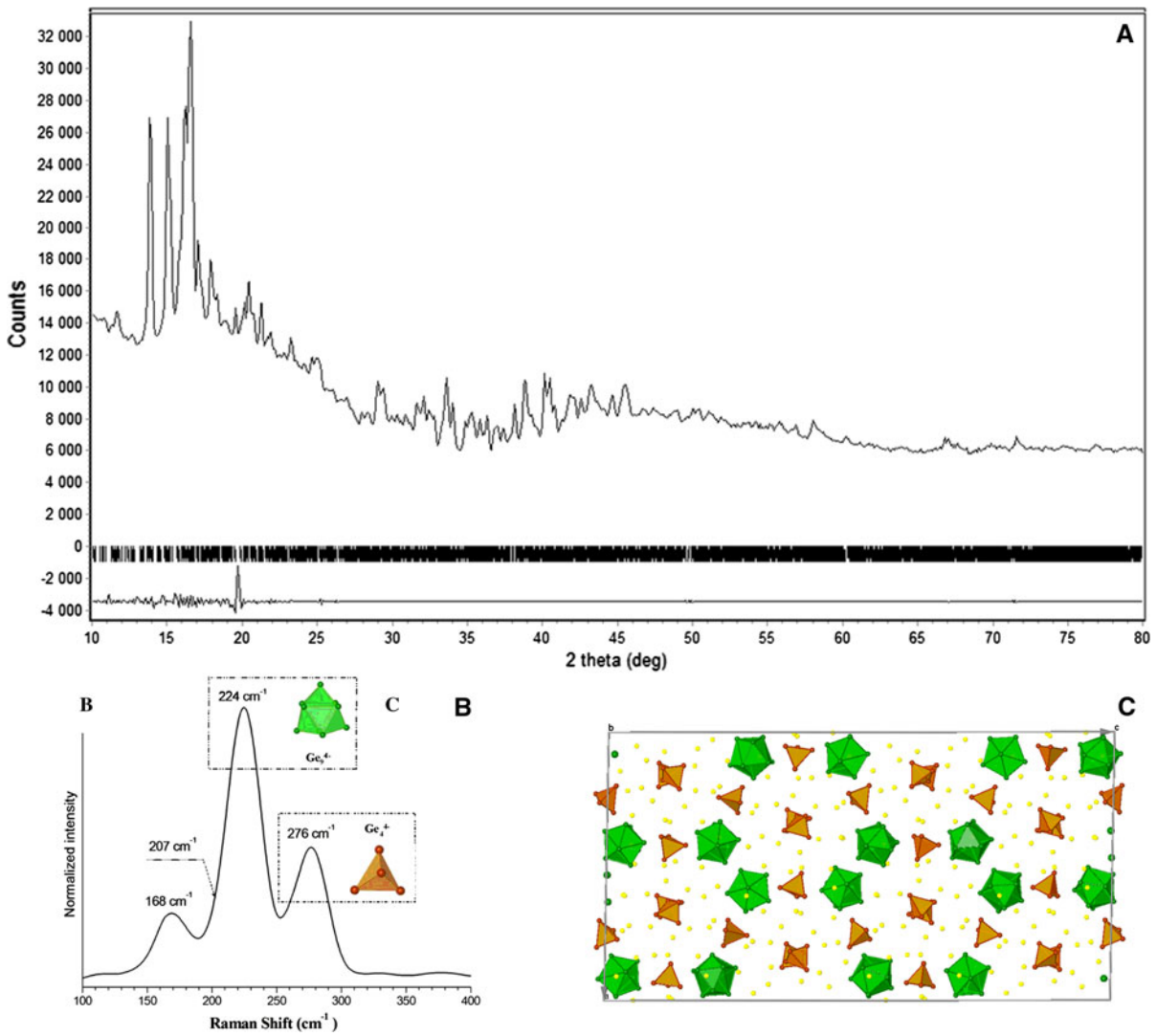

Fig. 2 X-ray diffractogram of $Na_{12}Ge_{17}$ (**a**), Raman spectrum of $Na_{12}Ge_{17}$ (**b**) and structure projection along *b* axis emphasizing the Ge_4^{4-} and Ge_9^{4-} anionic clusters (**c**)

224 cm^{-1} are characteristic of Ge_4^{4-} and Ge_9^{4-} clusters, respectively. The slight asymmetry of the band lying at 224 cm^{-1} is attributed to overlapping of the v_2 mode of Ge_4^{4-} (207 cm^{-1}) with the intense band of Ge_9^{4-} (222 cm^{-1}). Finally, the third band at 168 cm^{-1} is assigned to the v_3 vibration mode of Ge_4^{4-} (164 cm^{-1}) which overlaps with the Ge_9^{4-} vibration modes occurring in the same domain (188, 164, and 147 cm^{-1}). Raman spectroscopy brings information that, in addition to XRD results, allows the complete and unambiguous identification of compound $Na_{12}Ge_{17}$.

The route I solid–liquid reaction

The route I solid–liquid reaction is carried out using solid $Na_{12}Ge_{17}$ and either benzyl alcohol or butanol as oxidizing agents. Powder XRD analyses of products have shown that $Na_{12}Ge_{17}$ reacts completely during the oxidation reaction. In all cases, products of reaction are crystalline as proved by the electron diffraction patterns indexed within the cubic diamond-type structure of germanium (JCPDS files no. 04-0545, $a = 5.657$ Å).

As clearly illustrated in Fig. 3, particle size depends on the nature of the oxidizing agent: small NPs of 5.4 ± 2.3 nm in diameter are obtained from benzyl alcohol while particles of 19.1 ± 8.5 nm in diameter, with a larger size distribution, are obtained from butanol. In the following, these samples will be referred to as 5 and 20 nm NPs.

Raman spectroscopy has proven its efficiency to characterize these materials, even those being poorly crystallized or amorphous. Actually, Raman lines are characterized by their shape (width, symmetry) and their position, parameters that are strongly correlated with the structure/morphology (crystalline, amorphous) and with the particle size (micrometric, nanometric).

Germanium nanopowders from route I reactions are analyzed by Raman spectroscopy. Their spectra, shown in Fig. 4, present a large and asymmetric band clearly shifted from the position of the Raman line attributed to crystalline germanium (Ge–Ge stretch at 302 cm^{-1}). The Raman band position is dependent on the particle size, shifted toward low wavenumbers when the average particle size decreases, and broadened when the amorphous character increases (Muthuswamy et al. 2013; Schlecht et al. 2004; Gorokhov et al. 2005). After background correction, the experimental Raman spectrum is fitted using two Gaussian functions centered at 278 and 261 cm^{-1} (sample from benzyl alcohol). The contribution at 278 cm^{-1} is attributed to the crystalline core of the particles while that at 261 cm^{-1} corresponds to the amorphous part of the sample (surface and/or amorphous NPs). For samples prepared in butanol, Gaussian parameters are found slightly closer to values for bulk Ge, the Raman shifts of 288 and 271 cm^{-1} are in agreement with an increase in the coherence length of the particles crystalline core. These values of Raman shifts can be compared with 273 cm^{-1}, a value reported for nanocrystals (Ma et al. 2008).

The route II liquid–liquid reaction

Ge-nanosized samples are also prepared by the liquid–liquid route II reaction, which proceeds through the

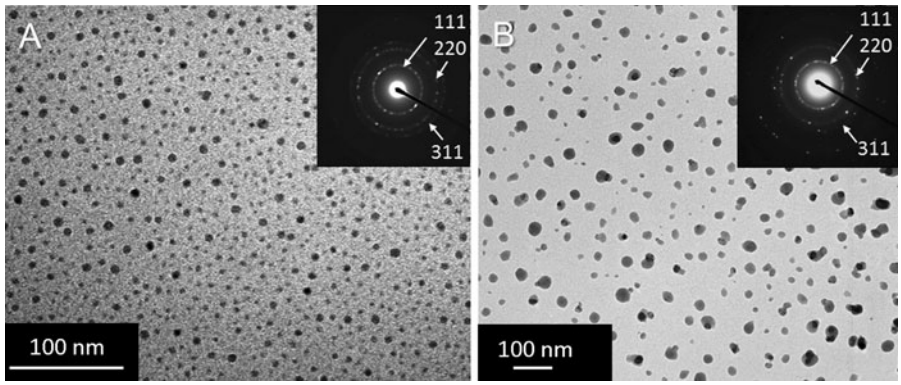

Fig. 3 TEM micrographs of crystalline Ge nanoparticles from route I using benzyl alcohol (**a**) and butanol (**b**) as oxidizing agent (*insets* SAED)

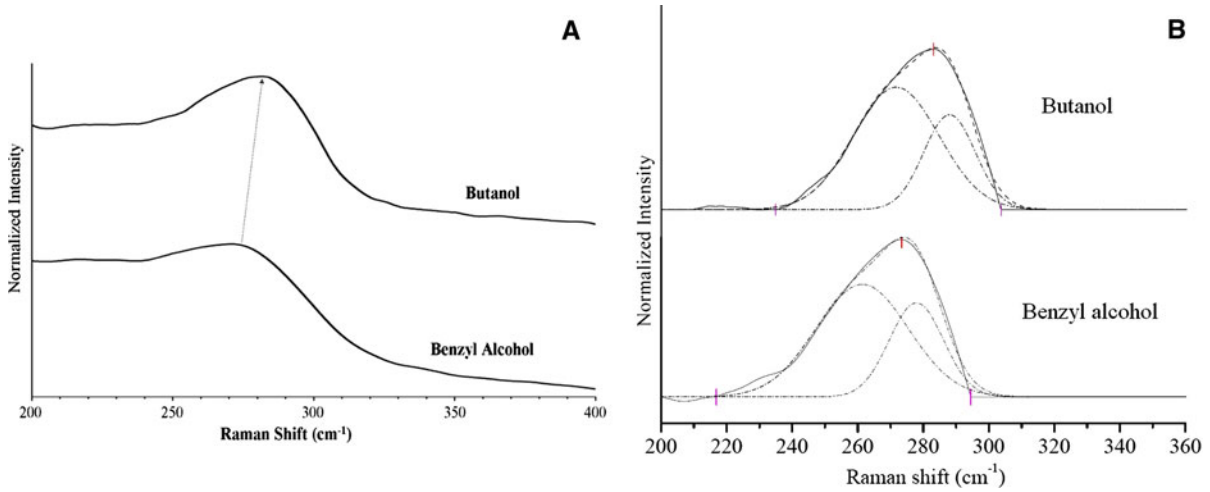

Fig. 4 **a** Raman spectra of Ge nanopowders illustrating the increase in Raman shift (from benzyl alcohol to butanol). **b** Fitted spectra after background correction

solubilization in ethylenediamine of the $Na_{12}Ge_{17}$ Zintl phase prior to oxidation. In that case, the individualized Ge_4^{4-} and Ge_9^{4-} Zintl units already present in the solid state are released as free anionic species in the solution. The intense brown–violet color of the solution was indicative of the presence of Ge anionic clusters able to react immediately with the alcohol. The route II reaction takes place in specific conditions (kinetics, mechanism,…) that might be significantly different from route I reaction conditions.

Powders obtained in that way with benzyl alcohol or butanol are studied using Raman spectroscopy. The recorded spectra, typical of Ge nanosized particles, showed large and asymmetric bands with Raman shifts of 264 cm^{-1} (benzyl alcohol) and 273 cm^{-1} (butanol). The displacement of the band from 264 to 273 cm^{-1} may be interpreted as the consequence of an increase in the long-distance order within the material, associated with a particle size enlargement or/and a crystallinity improvement. Comparison with the Raman shifts (278 and 288 cm^{-1}) observed for route I products indicates that route II products displayed a shorter coherence length.

Sample morphology and particle size distribution are examined by electron microscopy, the TEM micrographs of two samples prepared from benzyl alcohol and butanol are given comparatively in Fig. 5.

Whatever oxidizing agent is used, individualized NPs are found embedded in an amorphous germanium matrix. With benzyl alcohol, particles are below 7 nm in diameter and amorphous; while with butanol, crystalline particles range between 10 and 15 nm. The difference in morphology between routes I and II products may be attributed to the ability of Zintl anions to react with the alcohol. In the route I reaction, the Zintl anionic units (Ge_4^{4-} and Ge_9^{4-}) confined in the solid phase would react rather slowly with the alcohol. Instead, in the route II reaction, these units already present in the solution are immediately available for reaction with alcohol, leading to embedded NPs.

Results acquired from microscopy well agree with findings from Raman spectroscopy and XRD. In route II experiments, as already observed for route I, light alcohols are the most reactive oxidizing agents. Butanol is found to react faster than benzyl alcohol and to produce larger particles with higher crystallinity. The exothermic character of the reaction causes a local elevation of temperature, a factor that could favor the crystallization of Ge particles.

The route III reaction

In order to avoid the Zintl-phase high-temperature synthesis, elements are directly mixed in ethylenediamine. Though soluble in ethylenediamine, some solid germanium is still present at the bottom of the reactor after stirring the solution during 3 days. The dark-violet coloration of the solution indicated the presence of germanium anions. After filtration, the solution is added to benzyl alcohol or butanol to perform the

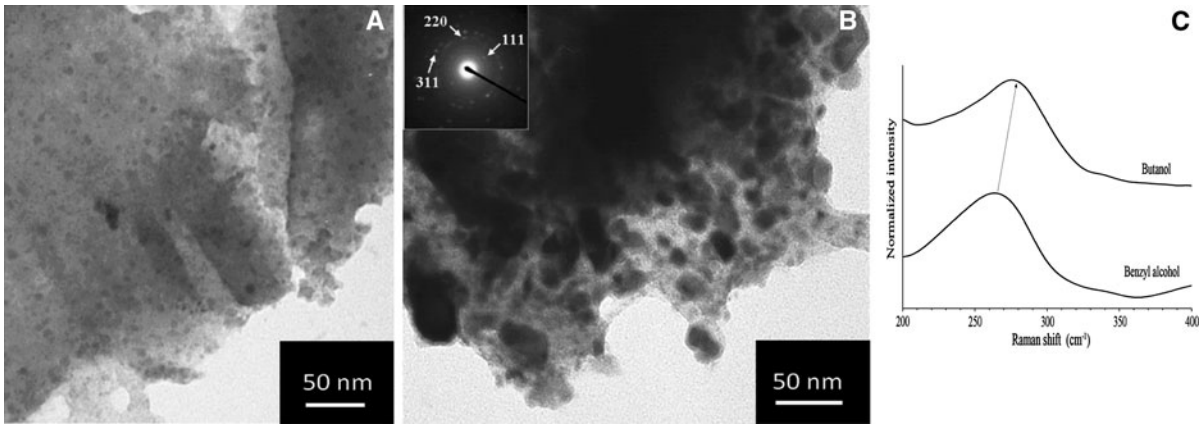

Fig. 5 TEM micrographs of Ge nanoparticles obtained from route II in benzyl alcohol (**a**) and butanol (**b**), Raman spectra of the corresponding materials (**c**)

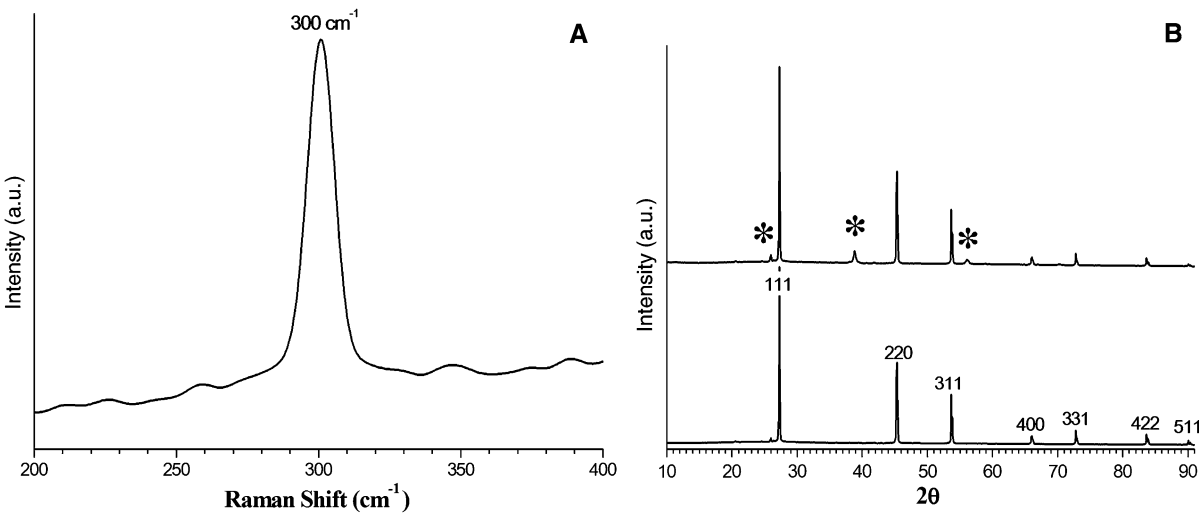

Fig. 6 Raman spectrum for a sample from route III with benzyl alcohol (**a**) and its XRD powder pattern indexed with cubic Ge (**b**)

oxidation reaction. No effect related to the nature of the alcohol can be detected.

The black powder collected, washed, and dried is analyzed by XRD, its pattern indicated the presence of a small quantity of a sodium hydrogen germanium oxide hydrate, identified as $Na_3HGe_7O_{16}(H_2O)_4$ (ICDD no. 01-076-0102), in addition to crystallized Ge. Diffraction lines marked with a star correspond to the germanium hydrate (Fig. 6b).

The presence of germanium hydrate supports the proposed mechanism: Ge anionic clusters can be oxidized either to Ge in anhydrous conditions or to sodium hydrogen germanium oxide hydrate in the presence of residual water (several ppms). The hydrate is easily eliminated by acid wash with dilute nitric acid. Unlike powders from routes I and II, the Ge powder from route III displays very narrow XRD lines suggesting the presence of large crystalline particles. The Raman band is observed at 300 cm^{-1}, the same position as for Ge commercial powder (150 μm). Nevertheless, with a half-maximum full-width of 11 cm^{-1} instead of 4 cm^{-1}, the band is slightly wider. The asymmetry would be assigned to a non-homogeneous size distribution and broadening explained by a reduction in the particle size.

These interpretations are consistent with the large crystalline aggregates of 50–100 nm observed in TEM images for samples prepared either from benzyl

alcohol or from butanol (not shown). The observed particle size in product is at least two orders of magnitude below the powder used as reagent, another argument for the reaction mechanism proposed. At first sight, the routes II and III reactions would appear very similar. Nonetheless, they are quite different since their final products do not display close characteristics. It is likely that solubilization in ethylenediamine of $Na_{12}Ge_{17}$ on one hand, and Na and Ge (in 12/17 atomic proportions) on the other hand, do not produce identical solutions. Raman studies of these solutions could indicate which species were present in the solutions, but they do not give workable data. Finally, no conclusive proof of the formation of Ge Zintl anions in the solution can be provided, anyway consideration of results from route III stresses the need to retain the high-temperature synthesis of the Zintl phase and underlines how complex the reaction media could be.

Raman spectra and samples stability

For each sample, Raman spectra are first acquired using the lowest intensity for the laser beam (50 μW, D2 filter), and then the intensity can be increased to 75 μW (D1) or 200 μW (D0.6). Depending on experimental conditions, a displacement of the Raman bands is observed that could be correlated with the sample stability under irradiation. To better understand the origin and try to quantify the amplitude of such displacements, Raman experiments are performed for Ge wafers and Ge commercial powder. For these two samples, Raman lines occur at 300 cm^{-1} in the first spectrum recorded with the lowest intensity (D2 filter).

As shown in Fig. 7, a progressive increase of the beam intensity using successively D1 and D0.6 filters does not induce any change in the band position for the Ge wafer. Instead, the Raman band of the Ge powder is continuously shifted toward weak displacement, as the beam intensity is increased (D1 then D0.6 filter). After a subsequent intensity lowering (D2 filter), the Raman line recovers its initial position. A similar phenomenon has been reported for small silicon crystalline nanowires of about 2 nm in diameter (Gupta et al. 2003). This reversible event results from thermal expansion: crystal cell inflates with the elevation of local temperature due to the beam energy and then contracts upon cooling. In the meantime, the Raman band shifts to low displacement and retrieves its initial position. This effect is only observed for powders and then called "powder effect." Owing to higher structural constraints, it does not occur for Ge wafers. This phenomenon, sensitive to the sample morphology, would be also associated with a decrease in thermal conductivity caused by the weakening of inter-grain contacts in finely divided powdered samples.

Similar experiments are carried out with the nano-sized Ge powders prepared in this work. As expected, the Ge powder obtained from route III reaction, composed of large particles of ~100 nm, gives rise to the powder effect, like the commercial powder.

The Raman band (D2 filter) of particles prepared from route I in benzyl alcohol is very intense (Figs. 4, 7). This intensity is characteristic of a loss in the long-distance order that causes suppression of the selection rules and allows all phonons participation (Richter et al. 1981). The raise in intensity occurs together with a

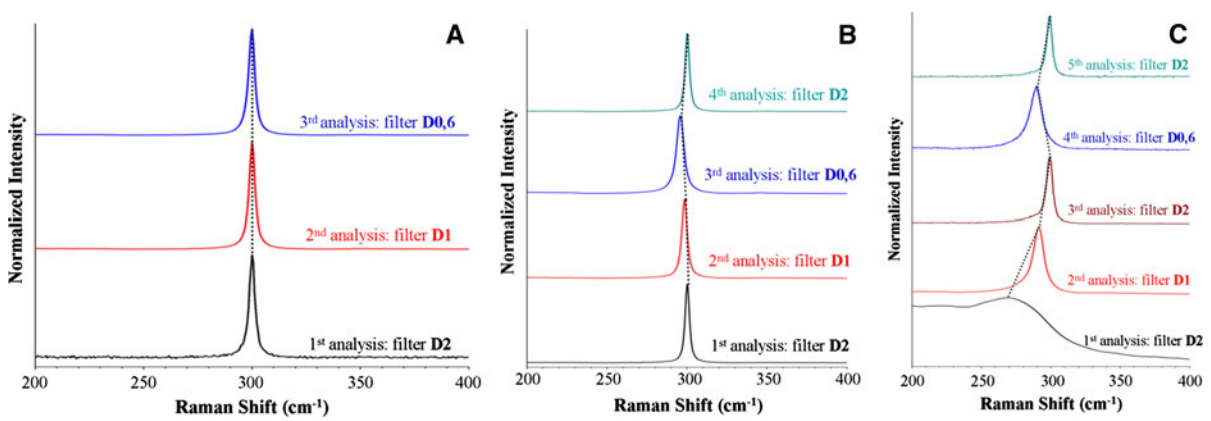

Fig. 7 Raman spectra under different irradiations for Ge wafers (**a**), Ge commercial powder (**b**), 5-nm Ge nanocrystals from route I (**c**)

narrowing of the band strongly moved toward high displacement values, sign of some local ordering (coalescence/crystallization). After a subsequent come back to low intensity (D2 filter) the band is observed at 300 cm^{-1} (Fig. 7). Based on results previously reported for silicon with shifts increasing with the particle size (Iqbal et al. 1980; Morhange et al. 1979), this irreversible phenomenon is assimilated to a thermal annealing.

Particles prepared from route II (16 h reaction) display a Raman band at 300 cm^{-1}, which shifts reversibly to low displacements demonstrating a powder effect. In case of powders collected after only 2 h of reaction (smaller amorphous particles), displacements of the Raman band initially occurring at 264 cm^{-1} indicate that the material first undergoes a thermal annealing and then a powder effect.

Electrochemical experiments

The Ge powders prepared in the present work are tested against a pure lithium electrode in electrochemical cells. Starting with a discharge of the battery, the maximum lithium insertion that can be achieved led to nominal compositions $Li_{4.2}Ge$ and $Li_{3.4}Ge$ for, respectively. small particles (5 nm) from benzyl alcohol and large particles (20 nm) from butanol, corresponding to the respective specific capacities of 1,530 and 1,250 mAh g^{-1} (Fig. 8). The limits in stoichiometry reached at the end of the subsequent charges of the cells are $Li_{1.7}Ge$ and $Li_{1.2}Ge$, leading to irreversible capacities of 600 and 380 mAh g^{-1} that would include solid–electrolyte layer occurring at first discharge. The reversible specific capacity for the complete first cycle is then about 900 mAh g^{-1} but the capacity rapidly fades upon cycling.

The voltage versus composition curves are represented in Fig. 8 for the first cycles of galvanostatic experiments. The first discharge is characterized by a pseudo plateau representing the continuous insertion of Li^+ into the electrode (Graetz et al. 2004). After the expected and usual small insertion of lithium in carbon black around 0.75 V, the Li insertion in Ge particles proceeds through two distinct processes better visualized in the derivative plots dx/dV as two peaks occurring at 0.35 and 0.18 V (Fig. 8a). During the

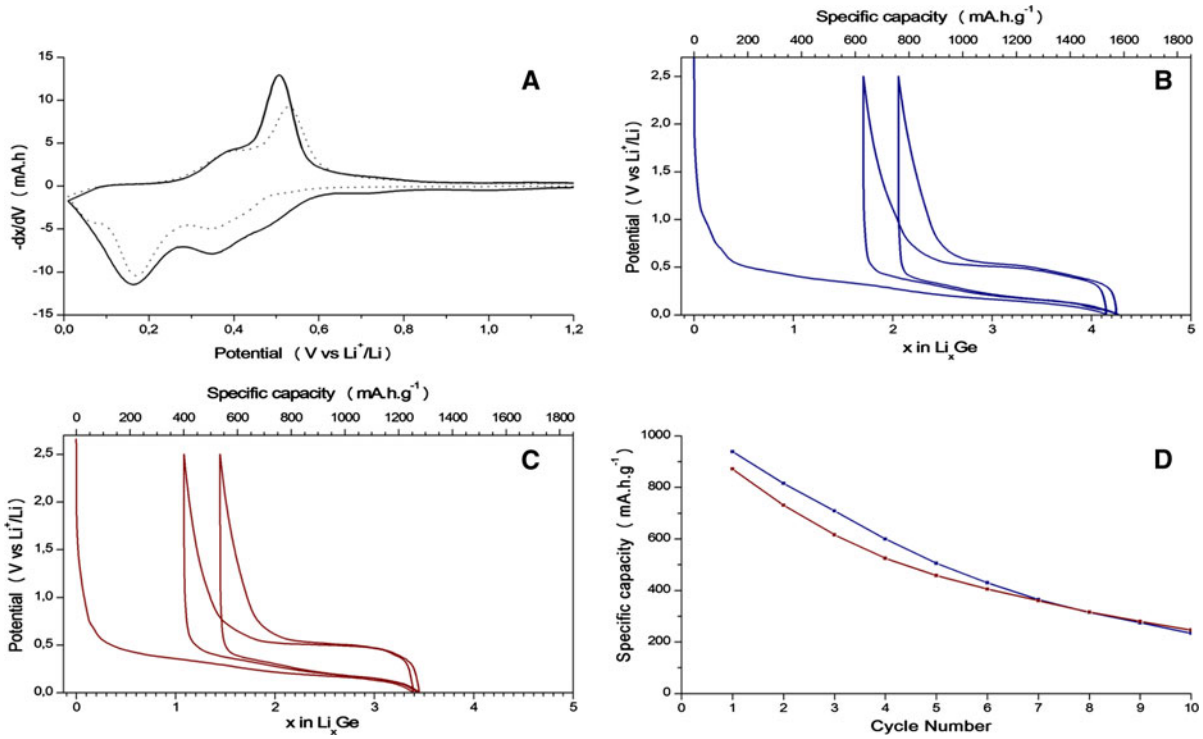

Fig. 8 Derivative plot dx/dV of small (*plain line*) and large (*dotted line*) particles (**a**), specific capacity for large (**b**) and small particles (**c**). **d** Comparative cycling performances

following charge, the large and intense peak observed at 0.5 V is associated with lithium extraction. The insertion mechanism of Li in small particles looks more complex, as attested by the additional and not fully separated peaks observed at 0.5 V in discharge and at 0.4 V in charge on potential derivative plots (Fig. 8a).

Despite quite good initial specific capacities, the initial capacity rapidly fades after 10 discharge/charge cycles. Such loss is often encountered for lithium insertion into electrochemically active materials as long as experimental conditions have not been optimized. The factors commonly mentioned to account for cycling degradation are the drop in electric conductivity due to electrode damage upon cycling and the side reactions with electrolyte that are enhanced by large surface areas of highly divided materials.

Li insertion into larger particles of 50–100 nm prepared from route III also occurs through a pseudo plateau up to a maximum of $\sim 4\ Li^+$ inserted per Ge, leading to a specific capacity of 1,405 mAh g^{-1}. The subsequent charge does not allow the extraction of the total Li amount, thus the electrode shows a rather large irreversible capacity of 510 mAh g^{-1}. Nevertheless, the capacity retention is found around 60 % over 10 cycles, which is much better than in case of small particles.

These exploratory experiments clearly evidence that the electrochemical behavior is related to the structure/morphology of the electro-active material. Small-sized particles are found not only to improve the initial capacities but also to increase the irreversible part of the capacity while larger particles are favorable to good capacity retention upon cycling. In these nanosized Ge materials, lithium insertion occurs through a continuous process without steps corresponding to the formation of intermediate intermetallic compounds. Improvement of the electrochemical performances would be reached by finding a compromise and optimizing the particles size. On the other hand, materials conditioning and experimental parameters need to be refined (binder, conducting matrix, exchange rate, potential windows,…) to improve the characteristics and the cycling lifetime of these batteries.

Initial capacities reach without any optimization vary from 1,250 to 1,530 mAh g^{-1}, not so far from the theoretical capacity of 1,600 mAh g^{-1} calculated for the nominal composition $Li_{22}Ge_5$. These capacities are in the same range as initial capacities reported in the literature for other kinds of nanosized germanium (Graetz et al. 2004) like Ge nanowires with an initial capacity of 1,141 mAh g^{-1} retained over 20 cycles (Chan et al. 2008). Ge amorphous NPs display a capacity of 1,470 mAh g^{-1}(Lee et al. 2005) while after annealing, the resulting crystallized particles inserted in a carbon matrix display a capacity of 1,200 mAh g^{-1} of which 88 % is retained over 30 cycles (Lee et al. 2007).

Conclusion

Nanostructured Ge powders are prepared using three different routes; the two first routes are based on the oxidization by an alcohol of a Zintl phase used as Ge precursor. The third route consists in the in situ Zintl anions formation and oxidation. Results clearly emphasize the crucial and unique role of the Zintl phase as a precursor of small-sized Ge NPs. One-phase reactions (route II) allow preparing crystalline particles embedded in amorphous matrix while two-phase reactions (solid/liquid, route I) yield well-defined isolated NPs. The difference in the product morphology may depend on the ability of the Zintl anions Ge_4^{4-} and Ge_9^{4-} to react with the alcohol. The free anions in the liquid phase ($Na_{12}Ge_{17}$/ethylenediamine solution) react more quickly than the anions frozen in the solid $Na_{12}Ge_{17}$ Zintl phase.

The results obtained in the present work show that the size of Ge NPs could be tuned by changing the chain length of the oxidizing agent, butanol and benzyl alcohol leading, respectively, to 5 and 20 nm NPs.

The Ge NPs prepared using these original oxidation reactions are free of organic residues and, when tested in electrochemical cells, exhibited initial capacities up to 1,530 mAh g^{-1} with a capacity retention reaching 60 %. These results are interesting for Ge anodic materials prepared by solution-phase chemistry insofar and could be greatly improved by optimization of the electrode preparation.

References

Armand M, Tarascon J-M (2008) Building better batteries. Nature 451:652–657

Armatas GS, Kanatzidis MG (2006a) Hexagonal mesoporous germanium. Science 313:817–820

Armatas GS, Kanatzidis MG (2006b) Mesostructured germanium with cubic pore symmetry. Nature 441(7097): 1122–1125

Bostedt C, van Buuren T, Willey TM, Franco N, Terminello LJ, Heske C, Möller T (2004) Strong quantum-confinement effects in the conduction band of germanium nanocrystals. Appl Phys Lett 84(20):4056

Chan CK, Zhang XF, Cui Y (2008) High capacity Li ion battery anodes using Ge nanowires. Nano Lett 8(1):307–309

Chiu HW, Kauzlarich SM (2006) Investigation of reaction conditions for optimal germanium nanoparticle production by a simple reduction route. Chem Mater 18(4):1023–1028

Chiu HW, Chervin CN, Kauzlarich SM (2005) Phase changes in Ge nanoparticles. Chem Mater 17:4858–4864

Chockla AM, Harris JT, Korgel BA (2011) Colloidal synthesis of germanium nanorods. Chem Mater 23(7):1964–1970

Chou NH, Oyler KD, Motl NE, Schaak RE (2009) Colloidal synthesis of germanium nanocrystals using room-temperature benchtop chemistry. Chem Mater 21(18):4105–4107

Collins G, Koleśnik M, Krstić V, Holmes JD (2010) Germanium nanowire synthesis from fluorothiolate-capped gold nanoparticles in supercritical carbon dioxide. Chem Mater 22(18):5235–5243

Fuller CS, Severiens JC (1954) Mobility of impurity ions in germanium and silicon. Phys Rev 96:21–24

Gerion D, Zaitseva N, Saw C, Casula MF, Fakra S, Van Buuren T, Galli G (2004) Solution synthesis of germanium nanocrystals: success and open challenges. Nano Lett 4(4):597–602

Gerung H, Bunge SD, Boyle TJ, Brinker CJ, Han SM (2005) Anhydrous solution synthesis of germanium nanocrystals from the germanium(II) precursor $Ge[N(SiMe_3)_2]_2$. Chem Commun 14:1914–1916

Gerung H, Boyle TJ, Tribby LJ, Bunge SD, Brinker CJ, Han SM (2006) Solution synthesis of germanium nanowires using a Ge^{2+} alkoxide precursor. J Am Chem Soc 128(15): 5244–5250

Goicoechea JM, Sevov SC (2005) Ligand-free deltahedral clusters of silicon in solution: synthesis, structure, and electrochemistry of $Si_9^{(2-)}$. Inorg Chem 44(8):2654–2658

Gorokhov EB, Volodin VA, Marin DV, Orekhov DA, Cherkov AG, Gutakovski AK, Shvets VA, Borisov AG, Efremov MD (2005) Effect of quantum confinement on optical properties of Ge nanocrystals in GeO_2 films. Semiconductors 39(10):1168–1175

Graetz J, Ahn CC, Yazami R, Fultz B (2004) Nanocrystalline and thin film germanium electrodes with high lithium capacity and high rate capabilities. J Electrochem Soc 151(5):A698

Gruttner A, Nesper R, Von Schnering HG (1982) Novel metastable germanium modifications *allo*-Ge and 4H–Ge from Li_7Ge_{12}. Angew Chem Int Ed 21(12):912–913

Guloy AM, Ramlau R, Tang Z, Schnelle W, Baitinger M, Grin Y (2006) A guest-free germanium clathrate. Nature 443: 320–323

Gupta R, Xiong Q, Adu CK, Kim UJ, Eklund PC (2003) Laser-induced Fano resonance scattering in silicon nanowires. Nano Lett 3(5):627–631

Hanrath T, Korgel BA (2002) Nucleation and growth of germanium nanowires seeded by organic monolayer-coated gold nanocrystals. J Am Chem Soc 124(7):1424–1429

Heath JR, Shiang JJ, Alivisatos AP (1994) Germanium quantum dots: optical properties and synthesis. J Chem Phys 101(2):1607

Henderson EJ, Hessel CM, Veinot JGC (2008) Synthesis and photoluminescent properties of size-controlled germanium nanocrystals from phenyl trichlorogermane-derived polymers received much attention over the past several decades, due in. J Am Chem Soc 130:3624–3632

Hoch C, Wendorff M, Rohr C (2003) Synthesis and crystal structure of the tetrelides $A_{12}M_{17}$ (A=Na, K, Rb, Cs; M=Si, Ge, Sn) and A_4Pb_9 (A=K, Rb). J Alloy Compd 361: 206–221

Iqbal Z, Webb P, Vepřek S (1980) Polycrystalline silicon films deposited in a glow discharge at temperatures below 250 °C. Appl Phys Lett 36(2):163

Kiefer F, Karttunen AJ, Döblinger M, Fässler TF (2011) Bulk synthesis and structure of a microcrystalline allotrope of germanium (*m-allo*-Ge). Chem Mater 23(20):4578–4586

Kliche G, Von Schnering HG, Schwarz M (1992) The internal vibrations of the tetrahetero–tetrahedrane anions Ge_4^{4-}, Sn_4^{4-}, and Pb_4^{4-}. Z Anorg Allg Chem 608:131–134

Kornowski A, Giersig M, Vogel R, Chemseddine A, Weller H (1993) Advanced laser technology. Adv Mater 5(9):634

Lambert TN, Andrews NL, Gerung H, Boyle TJ, Oliver JM, Wilson BS, Han SM (2007) Water-soluble germanium(0) nanocrystals: cell recognition and near-infrared photothermal conversion properties. Small 3(4):691–699

Lee H, Kim MG, Choi CH, Sun Y-K, Yoon CS, Cho J (2005) Surface-stabilized amorphous germanium nanoparticles for lithium-storage material. J Phys Chem B 109: 20719–20723

Lee H, Kim H, Doo S-G, Cho J (2007) Synthesis and optimization of nanoparticle Ge confined in a carbon matrix for lithium battery anode material. J Electrochem Soc 154(4):A343

Lee DC, Pietryga JM, Robel I, Werder DJ, Schaller RD, Klimov VI (2009) Colloidal synthesis of infrared-emitting germanium nanocrystals. J Am Chem Soc 131(10):3436–3437

Lu X, Ziegler KJ, Ghezelbash A, Johnston KP, Korgel BA (2004) Synthesis of germanium nanocrystals in high temperature supercritical fluid solvents. Nano Lett 4(5):969–974

Lu X, Fanfair DD, Johnston KP, Korgel BA (2005a) High yield solution–liquid–solid synthesis of germanium nanowires. J Am Chem Soc 127(45):15718–15719

Lu X, Korgel BA, Johnston KP (2005b) High yield of germanium nanocrystals synthesized from germanium diiodide in solution. Chem Mater 17(25):6479–6485

Ma X, Wu F, Kauzlarich SM (2008) Alkyl-terminated crystalline Ge nanoparticles prepared from NaGe: synthesis, functionalization and optical properties. J Solid State Chem 181:1628–1633

Medeiros-Ribeiro G, Bratkovski AM, Kamins TI, Ohlberg DAA, Williams RS (1998) Shape transition of germanium nanocrystals on a silicon (001) surface from pyramids to domes. Science 279:353–355

Min KS, Shcheglov KV, Yang CM, Atwater HA, Brongersma ML, Polman A (1996) The role of quantum-confined excitons vs defects in the visible luminescence of SiO_2 films containing Ge nanocrystals. Appl Phys Lett 68(18):2511

Morales AM, Lieber CM (1998) A laser ablation method for the synthesis of crystalline semiconductor nanowires. Science 279:208–211

Morhange JF, Kanellis G, Balkanski M (1979) Raman study of laser annealed silicon. Solid State Commun 31:805–808

Muthuswamy E, Iskandar AS, Amador MM, Kauzlarich SM (2013) Facile synthesis of germanium nanoparticles with

size control: microwave versus conventional heating. Chem Mater 25:1416–1422

Park M-H, Kim K, Kim J, Cho J (2010) Flexible dimensional control of high-capacity Li-ion-battery anodes: from 0D hollow to 3D porous germanium nanoparticle assemblies. Adv Mater 22(3):415–418

Richter H, Wang ZP, Ley L (1981) The one phonon Raman spectrum in microcrystalline silicon. Solid State Commun 39:625–629

Ruddy DA, Johnson JC, Smith ER, Neale NR (2010) Size and bandgap control in the solution-phase synthesis of near-infrared-emitting germanium nanocrystals. ACS Nano 4(12):7459–7466

Schlecht S, Yosef M, Fröba M (2004) Synthesis and Raman spectroscopy of nanoparticles of crystalline and X-ray amorphous germanium within mesoporous SiO_2. Z Anorg Chem 630(6):864–868

Somer M (2000) Vibrational spectra of the cluster anions $[E_4]^{4-}$ in the metallic sodium and barium compounds Na_4E_4 and Ba_4E_4 (E = Si, Ge). Z Anorg Allg Chem 626:2478–2480

Sun D, Riley AE, Cadby AJ, Richman EK, Korlann SD, Tolbert SH (2006) Hexagonal nanoporous germanium through surfactant-driven self-assembly of Zintl clusters. Nature 441:1126–1130

Tanke RS, Kauzlarich SM, Patten TE, Pettigrew KA, Murphy DL, Thompson ME, Lee HWH (2003) Synthesis of germanium nanoclusters with irreversibly attached functional groups: acetals, alcohols, esters, and polymers. Chem Mater 15(8):1682–1689

Taylor BR, Kauzlarich SM, Lee HWH, Delgado GR (1998) Solution synthesis of germanium nanocrystals demonstrating quantum confinement. Chem Mater 10:22–24

Taylor BR, Kauzlarich SM, Delgado GR, Lee HWH (1999) Solution synthesis and characterization of quantum confined Ge nanoparticles. Chem Mater 11(9):2493–2500

Taylor BR, Fox GA, Hope-Weeks LJ, Maxwell RS, Kauzlarich SM, Lee HWH (2002) Solution preparation of Ge nanoparticles with chemically tailored surfaces. Mater Sci Eng B 96(2):90–93

Vaughn DD, Bondi JF, Schaak RE (2010) Colloidal synthesis of air-stable crystalline germanium nanoparticles with tunable sizes and shapes. Chem Mater 22(22):6103–6108

Wang D, Dai H (2002) Low-temperature synthesis of single-crystal deposition. Angew Chem Int Ed 41(24):4783–4786

Wang D, Dai H (2006) Germanium nanowires: from synthesis, surface chemistry, and assembly to devices. Appl Phys A 85(3):217–225

Wang D, Chang Y-L, Liu Z, Dai H (2005) Oxidation resistant germanium nanowires: bulk synthesis, long chain alkanethiol functionalization, and Langmuir–Blodgett assembly. J Am Chem Soc 127:11871–11875

Wilcoxon J, Provencio P, Samara G (2001) Synthesis and optical properties of colloidal germanium nanocrystals. Phys Rev B 64:035417

Wu Y, Yang P (2000) Germanium nanowire growth via simple vapor transport. Chem Mater 12:605–607

Zaitseva N, Dai ZR, Grant CD, Harper J, Saw C (2007) Germanium nanocrystals synthesized in high-boiling-point organic solvents. Chem Mater 19(21):5174–5178